

# Comparison of Photovoltaic Module Performance Measurements

**A. Hunter Fanney**  
e-mail: Hunter.Fanney@nist.gov

**Mark W. Davis**

**Brian P. Dougherty**

National Institute of Standards and Technology,  
100 Bureau Drive,  
Gaithersburg, MD 20899-8632

**David L. King**

**William E. Boyson**

**Jay A. Kratochvil**

Sandia National Laboratories,  
PO Box 5800,  
MS 1033,  
Albuquerque, NM 87185-1033

*Computer simulation tools used to predict the energy production of photovoltaic systems are needed in order to make informed economic decisions. These tools require input parameters that characterize module performance under various operational and environmental conditions. Depending upon the complexity of the simulation model, the required input parameters can vary from the limited information found on labels affixed to photovoltaic modules to an extensive set of parameters. The required input parameters are normally obtained indoors using a solar simulator or flash tester, or measured outdoors under natural sunlight. This paper compares measured performance parameters for three photovoltaic modules tested outdoors at the National Institute of Standards and Technology (NIST) and Sandia National Laboratories (SNL). Two of the three modules were custom fabricated using monocrystalline and silicon film cells. The third, a commercially available module, utilized triple-junction amorphous silicon cells. The resulting data allow a comparison to be made between performance parameters measured at two laboratories with differing geographical locations and apparatus. This paper describes the apparatus used to collect the experimental data, test procedures utilized, and resulting performance parameters for each of the three modules. Using a computer simulation model, the impact that differences in measured parameters have on predicted energy production is quantified. Data presented for each module includes power output at standard rating conditions and the influence of incident angle, air mass, and module temperature on each module's electrical performance. Measurements from the two laboratories are in excellent agreement. The power at standard rating conditions is within 1% for all three modules. Although the magnitude of the individual temperature coefficients varied as much as 17% between the two laboratories, the impact on predicted performance at various temperature levels was minimal, less than 2%. The influence of air mass on the performance of the three modules measured at the laboratories was in excellent agreement. The largest difference in measured results between the two laboratories was noted in the response of the modules to incident angles that exceed 75 deg.*

[DOI: 10.1115/1.2192559]

## Introduction

The performance characteristics of photovoltaic modules are needed in order to model their annual performance [1–5]. Information available from manufacturers is typically limited to temperature coefficients, short circuit current  $I_{sc}$ , open circuit voltage  $V_{oc}$ , and the maximum power  $P_{max}$ , at rating conditions. This information, while useful in comparing photovoltaic module performance at rating conditions, is inadequate to predict annual performance under typical operating conditions [6–8]. It has been shown that the relative performance ranking at rating conditions may not agree with the ranking based on annual performance [9]. Discrepancies between the rated and annual rankings are attributed to the large annual variations that are experienced in incident angle, solar spectrum, operating temperature, and solar irradiance as compared to the typical rating conditions of 25 °C cell temperature, a prescribed solar spectrum, 1000 W/m<sup>2</sup> irradiance level, and zero angle of incidence.

During a multiyear study at National Institute of Standards and Technology (NIST), various photovoltaic modules have been integrated into a building's south-facing vertical façade [10,11]. During a typical year, the temperature of the photovoltaic cells

varied from –13 °C to over 75 °C, the air mass varied from 1.02 to 30, the solar irradiance varied from 0 W/m<sup>2</sup> to 600 W/m<sup>2</sup>, and the incident angle varied between 27 deg and 90 deg. As various photovoltaic modules respond differently to each of the parameters cited above, it is not surprising that the relative performance of photovoltaic modules exposed to actual operating conditions does not duplicate that obtained at a fixed set of rating conditions [9].

In order to accurately predict the annual performance of a photovoltaic system for any given geographical location, building orientation, and photovoltaic cell technology, models are needed that can accurately predict the response of the photovoltaic systems to the wide range of operational conditions they encounter. Sandia National Laboratories (SNL) has developed a photovoltaic array performance model [12] that is capable of predicting the annual electrical energy output of various photovoltaic modules to within 5% of the measured values [13]. The performance prediction methodology developed by SNL has been implemented in a personal computer program called PV Design Pro [14]. This model requires detailed input parameters that characterize the response of a given photovoltaic module to cell temperature, solar irradiance, incident angle, and air mass. In order to utilize PV Design Pro to predict the annual performance of modules used in the multiyear studies at NIST, module characterization parameters were measured at both NIST and SNL. This paper compares NIST and SNL electrical performance measurements for three photovoltaic modules.

Contributed by the Solar Energy Division of ASME for publication in the JOURNAL OF SOLAR ENERGY ENGINEERING. Manuscript received April 27, 2005; final manuscript received January 5, 2006. Review conducted by Antonio Marti. Paper presented at the 2005 International Solar Energy Conference (ISEC2005), August 6–12, 2005, Orlando, Florida.

**Table 1 Module specifications**

	Monocrystalline	Silicon film	Triple-junction amorphous
Cell technology	Monocrystalline	Silicon film	Triple-junction amorphous
Module dimensions (m × m)	1.38 × 1.18	1.38 × 1.18	1.37 × 1.48
Front cover	6 mm glass	6 mm glass	<sup>a</sup> Tefzel
Ethylene vinyl acetate encapsulant (EVA)	X	X	X
Backsheet/Color	Tedlar/Charcoal <sup>a</sup>	Tedlar/Charcoal <sup>a</sup>	Stainless steel
Cell dimensions (mm × mm)	125 × 125	150 × 150	119 × 340
Number of cells (in series)	72	56	44
Rated power (W)	153	92	128
Cell area (m <sup>2</sup> )	1.020	1.341	1.780
Aperture area (m <sup>2</sup> )	1.682	1.682	2.108
Coverage area (m <sup>2</sup> )	1.160	1.371	1.815

<sup>a</sup>Certain trade names and company products are mentioned in the test or identified in an illustration in order to adequately specify the experimental procedure and equipment used. In no case does such an identification imply recommendation or endorsement by the National Institute of Standards and Technology, nor does it imply that the products are necessarily the best available for the purpose.

## Experimental Apparatus

**Photovoltaic Modules.** The three photovoltaic modules in this study consisted of two custom fabricated and one commercially available module, Table 1. The custom fabricated modules were constructed using monocrystalline and silicon film cells and sized to replace existing fenestration units. The commercially available photovoltaic module utilized triple-junction amorphous silicon photovoltaic cells. Unlike the monocrystalline and silicon film modules, in which the number of cells can readily be varied to produce modules of various sizes, the manufacturing process used to produce triple-junction amorphous silicon modules is not readily amendable to producing a small quantity of custom sized modules. The total cell, coverage, and aperture areas listed in Table 1 represent the combined cell area, the combined areas of the cells and any spaces between the cells, and the total area of the module respectively. A detailed description of the modules is given in Fanney et al. [10].

**NIST and SNL Solar Tracking Test Facilities.** The mobile solar tracking facility at NIST used to characterize the electrical performance of building integrated photovoltaic (BIPV) modules is shown in Fig. 1. The facility incorporates meteorological instruments, a data acquisition system, and a current versus voltage (IV) curve tracer. Precision spectral pyranometers are used to measure

total (beam plus diffuse) solar radiation. A pyreheliometer is used to measure the beam component of solar radiation. Spectral radiation data from 300 nm to 1100 nm are obtained using a spectroradiometer with selectable scan intervals. A three-cup anemometer and wind vane assembly is used to measure wind speed and direction, respectively. Ambient temperature is measured using a perforated tip, type-T thermocouple sensor enclosed in a naturally ventilated multiplate radiation shield. The output signals of the meteorological instruments and thermocouples associated with the building integrated photovoltaic modules are measured using a 60-channel data acquisition system. An electronic ice point reference unit is used to reference the thermocouple junctions.

The IV curve tracer is programmed to sweep the module's IV curve and store the resulting values every minute. The current and voltage resolutions are 14 mV and 2.4 mA, respectively. The solar tracking test facility is powered by means of an on-board uninterruptible power supply (UPS) capable of operating the equipment for approximately 14 h. For multiple day tests, the UPS is charged through the use of a portable generator.

The electrical performance testing at SNL was done with the modules mounted on a computer controlled solar tracker, Fig. 2. Meteorological data instrumentation provided wind speed (three-cup anemometer at 3 m height), wind direction, pressure, and both ambient and dew point temperature using an aspirated shield. Total (global) solar irradiance data were provided by a silicon reference cell and a thermopile-based pyranometer mounted on the solar tracker, and simultaneous measurements from other facility instruments provided direct normal (beam) irradiance and total horizontal diffuse irradiance. All solar irradiance instruments have calibrations traceable to established standards organizations. Like NIST, the solar spectral content was measured in the wavelength range from 300 nm to 1100 nm using a spectroradi-

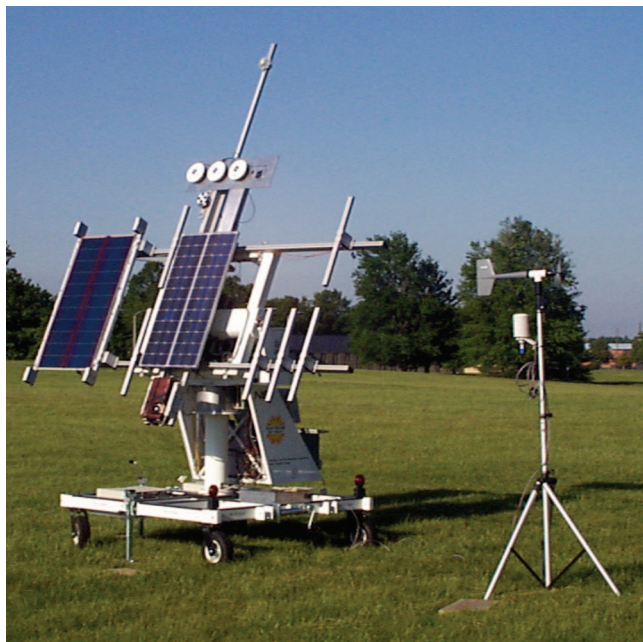


**Fig. 1 NIST's mobile solar tracking facility**



**Fig. 2 SNL's photovoltaic test facility**

**Table 2 Summary of measured photovoltaic module parameters**

Standard reference condition		Silicon film		Monocrystalline		Triple-junction amorphous		
		NIST Insulated	SNL Uninsulated	SNL Insulated	NIST Insulated	SNL Uninsulated	NIST Insulated	SNL Uninsulated
$P_{mpo}$	(W)	103.96	104.95	104.32	133.4	133.99	57.04	57.2
$I_{sco}$	(A)	5.11	5.07	5.04	4.37	4.32	4.44	4.48
$V_{oco}$	(V)	29.61	30.12	30.23	42.93	43.53	23.16	23.49
$I_{mpo}$	(A)	4.49	4.46	4.41	3.96	3.92	3.61	3.52
$V_{mpo}$	(V)	23.17	23.53	23.66	33.68	34.23	16.04	16.27
Module temperature coefficients								
$\alpha_{ISC}$	(A/°C)	4.68E-03	4.78E-03	4.78E-03	1.75E-03	1.50E-03	5.61E-03	6.58E-03
$\alpha_{ISC}$	(1/°C)	9.16E-04	9.40E-04	1.02E-03	4.01E-04	3.50E-04	1.26E-03	1.47E-03
$\alpha_{IMP}$	(A/°C)	1.60E-03	2.00E-03	2.00E-03	-1.54E-03	-1.72E-03	7.35E-03	7.50E-03
$\alpha_{IMP}$	(1/°C)	3.58E-04	4.46E-04	4.73E-04	-3.90E-04	-4.46E-04	2.03E-03	2.15E-03
$\beta_{VOC}$	(V/°C)	-1.30E-01	-1.41E-01	-1.41E-01	-1.52E-01	-1.74E-01	-9.31E-02	-1.04E-01
$\beta_{VOC}$	(1/°C)	-4.39E-03	-4.69E-03	-4.67E-03	-3.55E-03	-3.99E-03	-4.02E-03	-4.41E-03
$\beta_{VMP}$	(V/°C)	-1.30E-01	-1.40E-01	-1.40E-01	-1.54E-01	-1.76E-01	-4.77E-02	-5.07E-02
$\beta_{VMP}$	(1/°C)	-5.63E-03	-5.95E-03	-5.92E-03	-4.56E-03	-5.13E-03	-2.98E-03	-3.12E-03
Cell temperature coefficients								
$\alpha_{ISC}$	(A/°C)	8.36E-05	8.54E-05	8.54E-05	2.43E-05	2.08E-05	-	-
$\alpha_{IMP}$	(A/°C)	2.86E-05	3.57E-05	3.57E-05	-2.14E-05	-2.39E-05	-	-
$\beta_{VOC}$	(V/°C)	-2.32E-03	-2.52E-03	-2.52E-03	-2.11E-03	-2.42E-03	-	-
$\beta_{VMP}$	(V/°C)	-2.32E-03	-2.50E-03	-2.50E-03	-2.14E-03	-2.44E-03	-	-
Air mass coefficients								
f(AMa)	Cnst	9.38E-01	9.39E-01	9.31E-01	9.36E-01	9.25E-01	1.1	9.82E-01
	Ama	6.22E-02	5.52E-02	6.74E-02	5.43E-02	6.89E-02	-6.14E-02	5.88E-02
	Ama <sup>2</sup>	-1.50E-02	-1.09E-02	-1.69E-02	-8.68E-03	-1.39E-02	-4.43E-03	-3.73E-02
	Ama <sup>3</sup>	1.22E-03	8.13E-04	1.53E-03	5.27E-04	1.15E-03	6.32E-04	4.12E-03
	Ama <sup>4</sup>	-3.40E-05	-2.35E-05	-5.52E-05	-1.10E-05	-3.83E-05	-1.92E-05	-1.47E-04
Incident angle coefficients								
f(AOI)	Cnst	9.99E-01	1	1	1	1	1	1
	AOI	-6.10E-03	-2.44E-03	-2.44E-03	-5.56E-03	-2.44E-03	-5.65E-03	-5.02E-03
	AOI <sup>2</sup>	8.12E-04	3.10E-04	3.10E-04	6.53E-04	3.10E-04	7.25E-04	5.84E-04
	AOI <sup>3</sup>	-3.38E-05	-1.25E-05	-1.25E-05	-2.73E-05	-1.25E-05	-2.93E-05	-2.30E-05
	AOI <sup>4</sup>	5.65E-07	2.11E-07	2.11E-07	4.64E-07	2.11E-07	4.97E-07	3.83E-07
	AOI <sup>5</sup>	-3.37E-09	-1.36E-09	-1.36E-09	-2.82E-09	-1.36E-09	-2.74E-09	-2.31E-09
The following values of uncertainty represent the expanded uncertainty using a coverage factor of 2.								
NIST measurement uncertainties			SNL measurement uncertainties					
$P_{mpo} \pm 2.2\%$			$I_{sco} \pm 1.7\%$		$P_{mpo} \pm 2.3\%$		$I_{sco} \pm 1.9\%$	
$V_{oco} \pm 1.1\%$			$I_{mpo} \pm 1.6\%$		$V_{oco} \pm 1.0\%$		$I_{mpo} \pm 2.0\%$	
$V_{mpo} \pm 1.4\%$					$V_{mpo} \pm 1.1\%$			

ometer. Multiple small gage type-T thermocouples, with an electronic ice point reference mounted on the solar tracker, were used to measure back surface module temperature.

SNL's test facility had four separate systems for measuring module electrical characteristics, providing the opportunity for side-by-side outdoor testing of different module types. The IV curve sweep was generated using dc electronic loads. The programmable loads could be configured for power ranges from about 1 W to 1800 W using different plug-in cards. Simultaneous current and voltage measurements were obtained using a pair of precision autoranging voltmeters with resolution of 0.0035% of the measured value, or about 1 mV for a module voltage of 30 V.

**Measured Parameters**

Photovoltaic system simulation models require information that relates the electrical output of photovoltaic modules to various environmental and operating conditions. In this study the input information required by PV DESIGN PRO [14], a detailed simulation model using algorithms developed by King et al. [12,15-17] was measured using facilities at NIST and SNL. The required input information, Table 2, includes the effect of temperature, air mass, and incident angle on a module's electrical output as well as the electrical output at standard rating conditions. A description of each input parameter, the method of test used to obtain each parameter, and the measured results follow.

**Temperature Coefficients.** Temperature coefficients are used to quantify the relationship between various electrical characteristics of a photovoltaic device and its operating temperature. Unlike ASTM E 1036-02 [18] that utilizes only the short circuit temperature coefficients  $\alpha_{ISC}$  and the open circuit voltage temperature coefficient  $\beta_{VOC}$  to translate measured currents and voltages to various operating temperatures, the algorithms developed by King et al. [15] use two additional temperature coefficients, the maximum power current and voltage coefficients  $\alpha_{IMP}$  and  $\beta_{VMP}$ , respectively.

The procedure specified within ASTM E 1036-02 determines the open-circuit voltage and short-circuit current temperature coefficients from a matrix of open-circuit voltage and short-circuit current values that result from measurements over a range of operating temperatures of 0°C to 80°C and a specified irradiance, typically 1000 W/m<sup>2</sup>.

ASTM E 1036-02 allows measurements to be made using a pulsed indoor solar simulator, shuttered continuous solar simulator, shuttered sunlight, or continuous sunlight. Temperature coefficients for this study were determined outdoors at both laboratories using the methodology proposed by Sandia National Laboratories [12,15]. At NIST the back of each module was placed on a nominal 102 mm thick extruded insulation board that extends approximately 100 mm beyond the module's outer perimeter. At SNL the custom fabricated module using silicon film cells was insulated in an identical manner to the technique used at

NIST. The remaining two modules were tested at SNL without insulation present. Use of the insulation thermally insulates the photovoltaic module from the tracker's mounting structure and helps ensure temperature uniformity as well as increasing the temperature range to which the module is subjected during the temperature coefficient tests. Prior to testing, the module is shaded with a reflective cover positioned approximately 75 mm above the photovoltaic module.

The average temperature of each module is determined by the mean of five thermocouples attached to its rear surface. During the tests, the solar tracking facilities are operated in the full tracking mode, resulting in the sun's rays being perpendicular to the module's surface throughout the test. The cover used to shade the module is removed and data collection is initiated. The IV curve tracer at NIST captures the module's electrical performance each minute until the photovoltaic module's average temperature approaches steady state. The SNL current-voltage (IV) scans are measured at approximately 30 s intervals with the module held at the maximum-power point condition between scans.

At NIST the tests are conducted when the absolute air mass is as close as possible to the reference value of 1.5. The measured short-circuit current and maximum power current is adjusted by multiplying the measured values by the ratio of the reference irradiance  $E_0$  ( $1000 \text{ W/m}^2$ ) to the measured irradiance. The currents are subsequently adjusted to an absolute air mass ( $AM_a$ ) of 1.5 by using the measured air mass function for each module. At SNL temperature coefficient measurements are made during periods of low wind conditions and "stable" sunshine conditions, typically within an hour of solar noon. A spectral air mass correction is not applied to the SNL measured current values. The adjusted  $I_{sc}$  and  $I_{mp}$  for each IV curve are plotted against the average module temperature. The slopes of the resulting regressions are the temperature coefficients  $\alpha_{isc}$  and  $\alpha_{imp}$ .

The temperature coefficients for the open circuit and maximum power voltage are determined in a similar manner using the same set of IV curves. Unlike the short-circuit current and maximum power current, the voltage values are assumed to be independent of the solar irradiance level and air mass. King et al. [15] found that there is typically less than a 5% change in the voltage coefficients over a tenfold change in irradiance— $100 \text{ W/m}^2$  to  $1000 \text{ W/m}^2$ . The open circuit and maximum power voltage for each IV curve are plotted versus the module's temperature. The slope of the linear regressions relating the voltages to module temperature are the voltage temperature coefficients  $\beta_{voc}$  and  $\beta_{vmp}$ .

Table 2 includes a compilation of the temperature coefficients  $\alpha_{isc}$ ,  $\alpha_{imp}$ ,  $\beta_{voc}$ , and  $\beta_{vmp}$  measured at NIST and SNL in accordance with the previously described procedures. Two sets of units are associated with each coefficient. The test procedure produces results in units normally used within the photovoltaic industry  $A/^\circ C$  or  $V/^\circ C$ . Unfortunately, results presented in these units are not readily compared to temperature coefficients for modules that may use identical cells but differ in the number of cells or the manner in which the cells are interconnected. In order to address this issue and to facilitate comparisons, the current and voltage temperature coefficients are divided by the corresponding current or voltage values ( $I_{sc}$ ,  $I_{mp}$ ,  $V_{oc}$ , and  $V_{mp}$ ), at standard rating conditions. If the temperature coefficients of a photovoltaic module using identical cells but having a different electrical configuration are needed, the normalized temperature coefficients ( $1/^\circ C$ ) are multiplied by the appropriate value ( $I_{sc}$ ,  $I_{mp}$ ,  $V_{oc}$ , and  $V_{mp}$ ) of the module for which the coefficients are desired. Individual cell temperature coefficients for the silicon film and monocrystalline modules are also given in Table 2. The cell temperature coefficients for the triple-junction amorphous panel was not computed as each of the 22 triple-junction cells within this modules are comprised of three cells in series.

The temperature coefficients measured at NIST and SNL are presented in Figs. 3 and 4. It is interesting to note that although

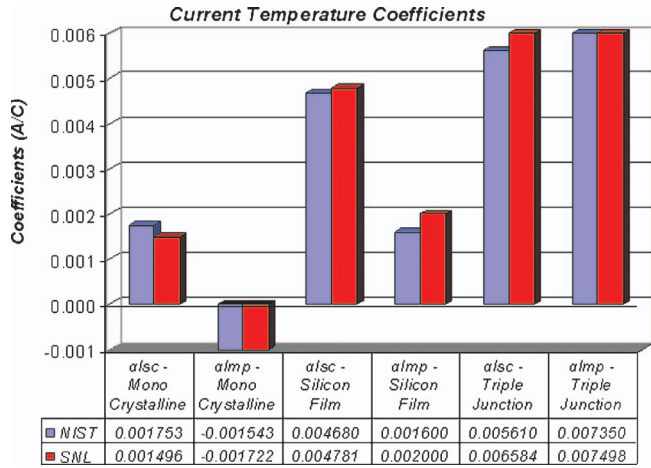


Fig. 3 Comparison of current temperature coefficients

the coefficients measured by the two laboratories vary from 2% to 17%, due to the small magnitude of the coefficients, the impact on predicted performance is insignificant. Table 3 illustrates this by taking the performance of the three modules at standard rating conditions, as reported by NIST in Table 2, and applying the temperature coefficients measured at the two laboratories to predict the performance of the modules at two extreme operating temperatures. The resulting difference between the predicted module performance parameters using the two sets of temperature coefficients is less than 3% in all cases.

**Air Mass Function.** The air mass function is an attempt to capture the influence of the solar energy's spectral distribution on the conversion efficiency of the photovoltaic cells. The solar spectrum is influenced by a number of factors including the absolute air mass, precipitable water content, turbidity, clouds, aerosol particle size distribution, particulate matter, and ground reflectance [19]. The magnitude of the solar spectrum's effect on the photovoltaic cell's performance depends upon the type of cell technology being utilized. King et al. [17] have found that under clear sky conditions, the majority of the solar spectral influence can be taken into account by considering only the air mass. The relationship between the photovoltaic module's short-circuit current and absolute air mass is defined as the air mass function.

The air mass function for each of the building integrated photovoltaic modules was measured using the methodology proposed by King et al. [12,17]. The NIST and SNL tracking facilities are

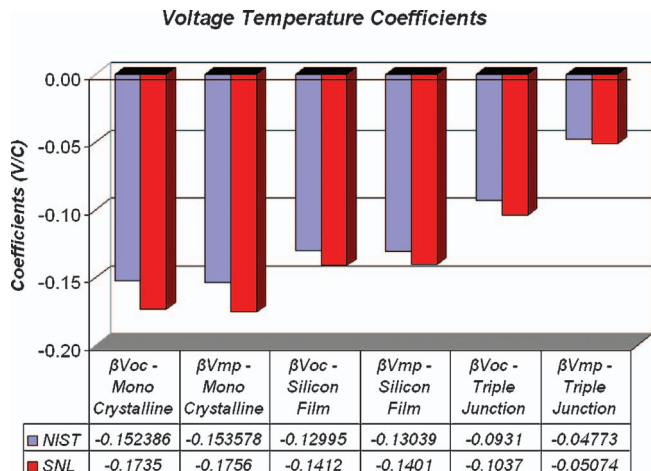


Fig. 4 Comparison of voltage temperature coefficients

**Table 3 Predicted electrical performance parameters using NIST and SNL temperature coefficients**

Module Temperature Coefficient Source	Monocrystalline				Silicon film				Triple-junction amorphous			
	0°C		75°C		0°C		75°C		0°C		75°C	
	NIST	SNL	NIST	SNL	NIST	SNL	NIST	SNL	NIST	SNL	NIST	SNL
$I_{sc}(A)$	4.33	4.33	4.46	4.44	4.99	4.99	5.34	5.35	4.30	4.28	4.72	4.79
$I_{mp}(A)$	4.00	4.00	3.88	3.87	4.45	4.44	4.57	4.59	3.43	3.42	3.98	3.99
$V_{oc}(V)$	46.74	47.27	35.31	34.26	32.86	33.14	23.11	22.55	25.49	25.75	18.51	17.98
$V_{mp}(V)$	37.52	38.07	26.00	24.90	26.43	26.67	16.65	16.17	17.23	17.31	13.65	13.50

operated in a manner that maintains a zero angle of incidence throughout the day. Measurements are made every minute at NIST and every 30 s at SNL from sunrise to sunset.

The short-circuit current associated with each IV curve is adjusted to a nominal temperature  $T_r$  of 25°C and nominal irradiance  $E_o$  of 1000 W/m<sup>2</sup> using the previously determined short-circuit temperature coefficient

$$I_{sc}(T_r, E_o) = \frac{E_o}{E} I_{sc}(T) + \alpha_{I_{sc}}(T_r - T) \quad (1)$$

The relative short-circuit values are subsequently obtained by dividing the values obtained using Eq. (1) by the temperature and irradiance adjusted short-circuit current measured at an absolute air mass of 1.5. The air mass is computed using the zenith angle of the sun  $Z_s$  and the following equation [20]:

$$AM = [\cos(Z_s) + 0.5057 \cdot (96.080 - Z_s)^{-1.634}]^{-1} \quad (2)$$

Finally, the absolute air mass is computed by multiplying the air mass value (Eq. (2)) by the product of the atmospheric pressure at the test site  $P$  to the atmospheric pressure at sea level  $P_o$ .

$$AM_a = AM \left( \frac{P}{P_o} \right) \quad (3)$$

A fourth-order regression is used to determine the relationship between the  $I_{sc}$  values determined in Eq. (1) and the corresponding absolute air mass values

$$f_1(AM_a) = a_0 + a_1 \cdot AM_a + a_2(AM_a)^2 + a_3(AM_a)^3 + a_4(AM_a)^4 \quad (4)$$

The resulting coefficients measured by the two laboratories for the various modules are given in Table 2.

It is interesting to note that the relative air mass response is similar for the modules that utilize the monocrystalline and silicon film cells. Air mass has a much greater effect on the triple-junction amorphous module than the other two modules, Fig. 5. At an absolute air mass of six, the response of the module using the triple-junction amorphous technology is approximately 70% of that exhibited by the (BIPV) modules using the monocrystalline and silicon film cell technologies. The significantly lower air mass response exhibited by the triple-junction amorphous module, is due to the fact that amorphous silicon cells are less responsive, compared to the other cell technologies, to the portion of the solar spectrum with wavelengths greater than 900 nm. As the absolute air mass increases, the solar spectrum contains a greater percentage of wavelengths above 900 nm resulting in the significant drop off exhibited in Fig. 5.

The predicted air mass function values using the coefficients measured at the two laboratories for the monocrystalline module agrees to within 1% for absolute air mass values of 4 or less and to within 4% for absolute air mass values having a value up to 9, Fig. 6. The predicted air mass values for the module utilizing triple-junction amorphous cells agrees to within 3% over the entire range.

SNL conducted two experiments to determine the air mass function for the silicon film module. One set of measurements was conducted with the extruded insulation applied to the rear surface of the module. The second set of measurements was captured with

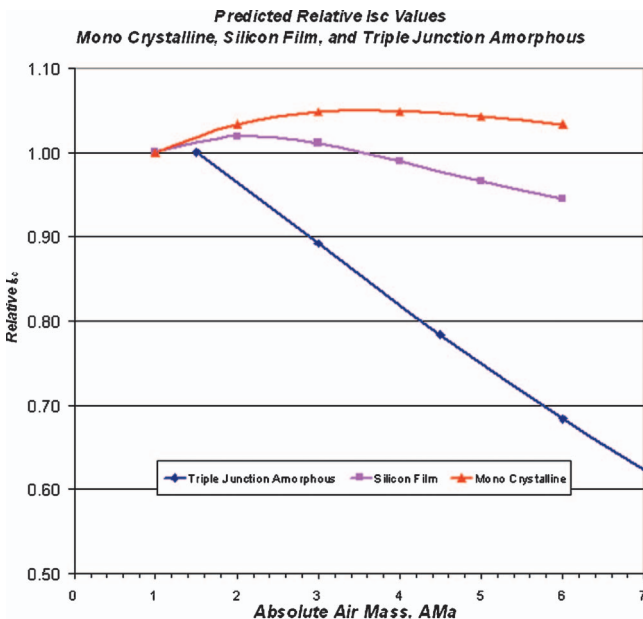


**Fig. 5 Air mass functions for modules**

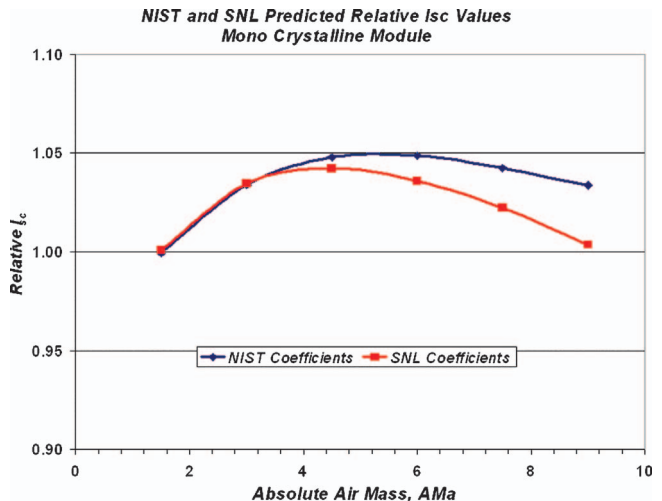


**Fig. 6 Comparison of air mass function values**

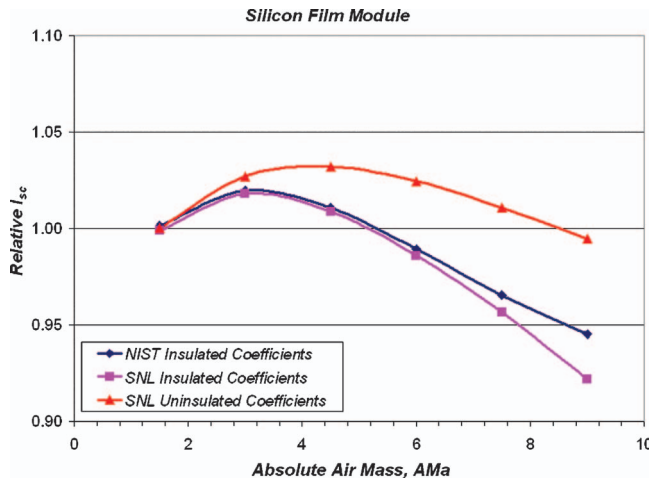


Fig. 7 Comparison of air mass functions for silicon film module

no insulation applied to the rear surface of the module. The results are compared to the NIST measurements, where insulation was present on the rear surface of the module, Fig. 7.

The resulting relative  $I_{sc}$  values predicted using the coefficients determined at SNL and NIST for the insulated silicon film module are within 1% over the entire air mass measurement range. It is interesting to note, Fig. 7, the unexpected difference in the predicted air mass function for the silicon film module in the insulated versus uninsulated SNL tests.

**Incident Angle Function.** The angle defined by the sun's rays and normal to the photovoltaic module's surface is the angle of incidence (AOI) or incident angle. The angle of incidence is computed using the sun's azimuth and zenith angles, and the slope and azimuth angles of the BIPV module [21]. The optical properties of the module's glazing material vary with incident angle. Under clear sky conditions, the "incident angle effect" can be quite pronounced for angles greater than 60 deg. Under uniform diffuse conditions, the angle of incidence does not affect the electrical output of the photovoltaic module. The reduction in annual performance of photovoltaic modules due to the varying incident angle has been described by Martin and Ruiz [22] for various geographical locations and tilt angles.

The effect of incident angle on the electrical performance of a photovoltaic module is described by an empirically determined function  $f_2$  (AOI) [12,17]. The NIST and SNL solar tracking facilities were used to vary the incident angles of the test modules while measuring its electrical performance. Data are collected at various incident angles with the greater emphasis on incident angles greater than 60 deg. A normal incidence pyreheliometer mounted on a separate solar tracker, provides independent measurements of the beam irradiance during these tests. The diffuse irradiance in the plane of the BIPV module is determined using the following equation:

$$E_{diff} = E_{tpoa} - E_{dni} \cos \theta \quad (5)$$

where  $E_{tpoa}$  is the total incident solar radiation, measured in the plane of the photovoltaic module using a precision spectral pyranometer,  $W/m^2$ ;  $E_{dni}$  is the beam irradiance measured using a normal incident pyreheliometer tracking the sun,  $W/m^2$ ; and  $\theta$  is the incident angle, deg.

The incident angle function value for each measurement is computed using the procedure developed by King et al. [12,17,23]

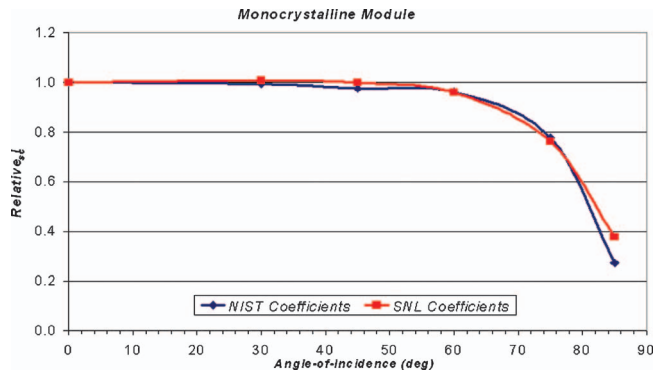


Fig. 8 Comparison of incident angle response functions for monocrystalline module

$$f_2(\text{AOI}) = \frac{\frac{E_o}{I_{sc0}} I_{sc}(\text{AM}_a = 1.5, T = 25^\circ \text{C}) - E_{diff}}{E_{dni} \cos(\text{AOI})} \quad (6)$$

where  $E_o$  and  $I_{sc0}$  are the reference irradiance and current output of the module at standard reporting conditions, respectively.

A fifth-order regression is used to determine the coefficients associated with the equation,

$$f_2(\text{AOI}) = b_0 + b_1 + \text{AOI} + b_2(\text{AOI})^2 + b_3(\text{AOI})^3 + b_4(\text{AOI})^4 + b_5(\text{AOI})^5 \quad (7)$$

The coefficients resulting from a fifth-order curve fit to the NIST and SNL incident angle data for each module are listed in Table 2. The incident angle responses to the monocrystalline and silicon film modules are very similar, Figs. 8 and 9, respectively. This is attributed to identical glazing material, 6 mm low-iron glass, used as the glazing material for both modules. The predictive relative  $I_{sc}$  values using the NIST and SNL coefficients for the single crystalline module are within 5% for incident angles up to 80 deg. At angles exceeding 80 deg the predicted  $I_{sc}$  values using the two sets of coefficients rapidly diverge. A comparison of the predicted  $I_{sc}$  values for the silicon film module shows agreement within 5% for angle of incidence up to 75 deg. As observed for the monocrystalline module, significant differences are observed for incident angles greater than 75 deg.

The triple-junction amorphous module uses a 0.05 mm (0.002 in.) thick Tefzel polymer glazing and its response to angle of incidence is significantly different than that observed for the

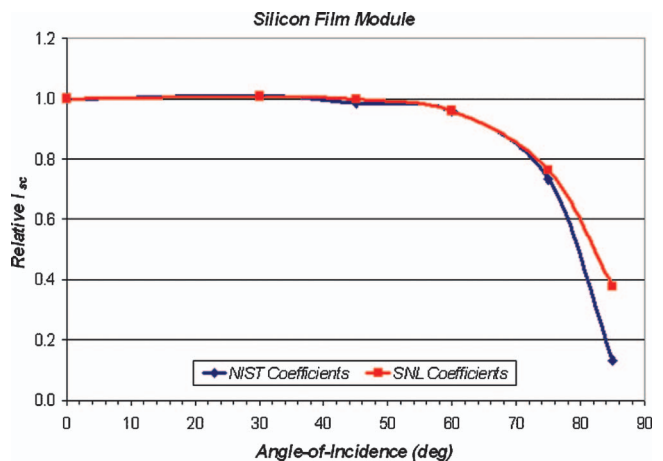
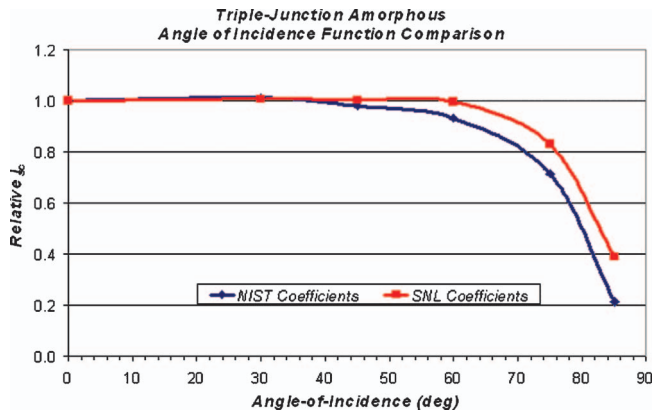


Fig. 9 Comparison of incident angle response functions for silicon film module



**Fig. 10 Comparison of incident angle response functions for triple-junction amorphous silicon module**

other two modules with a glass front surface, Fig. 10. Unlike the single crystalline and silicon film modules, the predicted relative  $I_{sc}$  values using the NIST and SNL coefficients begin to differ by approximately 10% at angles greater than 40 deg. At incident angles greater than 70 deg, significant differences are observed in the predicted  $I_{sc}$  values.

**Electrical Performance at Standard Rating Conditions.** A required input for photovoltaic performance models is the electrical performance of the photovoltaic module “standard reporting conditions.” Typically an irradiance level of  $1000 \text{ W/m}^2$ , a standard solar spectral distribution, a cell temperature of  $25^\circ\text{C}$ , and a 0 deg angle of irradiance are specified. These conditions have been adopted in this paper as the standard rating conditions with the exception of the standard solar spectrum. In the values reported within this paper, the photovoltaic modules’ performance reported by NIST is at an absolute air mass of 1.5. At SNL the solar spectrum is measured and used to correct the measured current values to the ASTM standard global spectrum [24] using the spectral response measurements for a representative solar cell and ASTM E 973-02 [25].

Each BIPV module’s performance at this set of rating conditions is determined using the procedures developed by King et al. [12]. Using the NIST and SNL solar tracking facilities to maintain the sun’s rays perpendicular to the front surface of the module (AOI=0), the curve tracer is used to collect IV curves under clear sky conditions. The resulting short-circuit current values are corrected to an absolute air mass of 1.5 and a  $25^\circ\text{C}$  cell temperature using the previously determined air mass function and temperature coefficients. The resulting  $I_{sc}$  values are plotted versus the coincident solar irradiance striking the module. A regression through the data is used to predict the short circuit current at  $1000 \text{ W/m}^2$ , denoted  $I_{sc0}$ .

The measured maximum power current values are plotted versus the effective irradiance defined as

$$E_e = \frac{I_{sc}}{I_{sc0}[1 + \alpha_{isc}(T_c - T_r)]} \quad (8)$$

where the denominator is the short-circuit current of the module at standard rating conditions adjusted to the reference temperature  $T_r$ . The maximum power current corresponding to an effective irradiance of unity is the maximum power current at standard rating conditions  $I_{mp0}$ .

Using the open-circuit and maximum power temperature coefficients, the open-circuit voltage and maximum power voltage measurements associated with each IV curve are translated to  $25^\circ\text{C}$  and plotted versus the natural logarithm of the effective irradiance values. Using a linear regression in the case of the open circuit voltage values, and a second-order polynomial in the case

**Table 4 Predicted January energy production Using NIST and SNL module parameters, kW h**

Monocrystalline		Silicon film		Triple junction	
NIST	SNL	NIST	SNL	NIST	SNL
10.61	10.62	7.54	7.51	5.29	5.24

of the maximum power voltage values, the open-circuit voltage and maximum power voltage values are determined at an effective irradiance of 1.0.

The current and voltage values for each photovoltaic module at standard reference conditions are given in Table 2. These values include the maximum power output  $P_{mp0}$ , the current and voltage at the maximum power point  $I_{mp0}$  and  $V_{mp0}$ , respectively, the short circuit current  $I_{sc0}$ , and the voltage at open circuit conditions  $V_{oc0}$ . The uncertainties associated with these measurements, included within Table 2, were computed in accordance with procedures outlined by Whitfield and Osterwald [26].

The agreement between the values reported by SNL and NIST is outstanding. It should be noted that this excellent agreement was achieved using different techniques at the two laboratories to measure incident solar radiation. NIST utilized a broadband thermopile pyranometer as the primary instrument to measure solar irradiance whereas SNL used a silicon reference cell with typical ASTM spectral corrections. The measured maximum power output at reference conditions is within 0.6% for all three modules. The two laboratories reported short-circuit and maximum power current values within 2% of each other, with the NIST reported values being slightly greater than those measured at SNL. Conversely, the values reported by SNL for open-circuit voltage and maximum power voltage were consistently larger than those measured at NIST, but always within 2%.

In order to better quantify the impact that the small differences in measured module parameters would have on the predicted performance of a photovoltaic system, NIST and SNL parameters were used in conjunction with a photovoltaic model [14] to predict the energy that would be produced by a single photovoltaic module system for the month of January in Gaithersburg, MD. Only the photovoltaic modules were modeled and it was assumed that they would be operated at their maximum power point. The modules were assumed to be used in a south-facing vertical wall application. Simulations were run for Gaithersburg, MD [27] using meteorological data recorded during January 2001. The results, Table 4, show that although small differences exist in the module parameters reported by the two laboratories, Table 2, the predicted energy production for each module, was in excellent agreement.

## Summary

The electrical performance of three photovoltaic modules was measured at the National Institute of Standards and Technology and Sandia National Laboratories. The objective was to compare the measured power output of the modules at standard rating conditions including the response of each module to changes in cell temperature, angle of incidence, and air mass under outdoor conditions. The study provided a comparison of measurements made under outdoor conditions at two facilities that differ in prevailing climatic conditions and experimental apparatus.

Although the temperature coefficients measured at the two laboratories varied from 2% to 17%, the impact of these differences on overall module performance was less than 2% for cell temperatures between  $0^\circ\text{C}$  and  $75^\circ\text{C}$ . The air mass functions, based on data from NIST and SNL, predicted relative short-circuit current values to within 4% for each of the three modules. The angle of incident functions measured at NIST and SNL for each of the modules was generally in good agreement for incident angles

of 70° or less. At incident angles that exceed 70°, significant differences were observed in the predicted  $I_{sc}$  values.

The performance of each module at standard rating conditions was determined using the procedure developed by King et al. [12,16]. The short circuit and maximum power current values reported by the two laboratories are within 2%, with the NIST reported values consistently greater than those reported by SNL. Conversely, the SNL reported values for open-circuit and maximum power voltages were consistently higher, approximately 2%, than the values determined at NIST. The power output at standard rating conditions was in excellent agreement, within 1%, for each of the three modules. Finally, the full set of NIST and SNL measured parameters, Table 2, were used in conjunction with a photovoltaic system model [14] to predict monthly energy production for the modules using meteorological data recorded during January 2001 at Gaithersburg, MD. The monthly energy production predicted using the parameters measured by the two different laboratories agreed to within 1% for all three modules.

## Acknowledgment

The authors greatly appreciate the financial support provided by Gerald Ceasar of NIST's Advanced Technology Program. The authors acknowledge Paula R. Svincek for preparing the manuscript, Andrew Heath for preparing the graphics, and Steven Bushey for running the computer model simulations. Sandia is a multiprogram laboratory operated by Sandia Corporation, a Lockheed Martin Company, for the United States Department of Energy's National Nuclear Security Administration under Contract No. DE-AC04-94AL85000.

## References

- [1] King, D. L., Boyson, W. E., and Kratochvil, J. A., 2002, "Analysis of Factors Influencing the Annual Energy Production of Photovoltaic Systems," Proceedings of the 29th IEEE Photovoltaic Specialists Conference, New Orleans, LA, May 20–24, pp. 1356–1361.
- [2] Marion, B., 2002, "A Method for Modeling the Current-Voltage Curve of a PV Module for Outdoor Conditions," *Prog. Photovoltaics* **10**, pp. 205–214.
- [3] Marion, B., Rummel, S., and Anderberg, A., 2004, "Current-Voltage Curve Translation by Bilinear Interpolation," *Prog. Photovoltaics* **12**, pp. 593–607.
- [4] Nakajima, A., Ichikawa, M., Kondo, M., Yamamoto, K., Yamagishi, H., and Tawada, Y., 2004, "Spectral Effects of a Single-Junction Amorphous Silicon Solar Cell on Outdoor Performance," *Jpn. J. Appl. Phys., Part 1 Part 1*, **43**(5A), pp. 2425–2531.
- [5] Kroposki, B., Marion, W., King, D. L., Boyson, W. E., and Kratochvil, J., 2002, "Comparison of Module Performance Characterization Methods for Energy Production," Paper No. NREL/TP-520-29245.
- [6] Marion, B., Kroposki, B., Emery, K., del Cueto, J., Myers, D., and Osterwald, C., 1999, "Validation of a Photovoltaic Module Energy Ratings Procedure at NREL," Paper No. NREL/TP-529-26909.
- [7] Gay, C. F., Rumberg, J. E., and Wilson, J. H., 1982, "AM-PM: All Day Module Performance Measurements," *Proc. 16th IEEE Photovoltaic Specialist*

- Conf., San Diego, IEEE New York, pp. 1041–1046.
- [8] Firor, K., 1985, "Rating PV Systems," *Proc. 18th IEEE Photovoltaic Specialist Conference*, Las Vegas, NV, October, pp. 1443–1448.
- [9] Fanney, A. H., Dougherty, B. P., and Davis, M. W., 2002, "Performance and Characterization of Building Integrated Photovoltaic Panels," *Proc. 29th IEEE Photovoltaic Specialists Conference*, (CD-ROM) New Orleans, LA, May 20–24.
- [10] Fanney, A. H., Dougherty, B. P., and Davis, M. W., 2001, "Measured Performance of Building Integrated Photovoltaic Panels," *Sol. Energy*, **123**, pp. 187–193.
- [11] Dougherty, B. P., Fanney, A. H., and Davis, M. W., 2005, "Measured Performance of Building Integrated Photovoltaic Panels-Round 2," *Sol. Energy*, **127**, pp. 314–323.
- [12] King, D. L., Boyson, W. E., and Kratochvil, J. A., 2004, "Photovoltaic Array Performance Model," Sandia Report No. SAND 2004-3535.
- [13] Davis, M. W., Fanney, A. H., and Dougherty, B. P., 2002, "Evaluating Building Integrated Photovoltaic Performance Models," *Proc. 29th IEEE Photovoltaic Specialists Conference*, (CD-ROM) New Orleans, LA, May 20–24.
- [14] PV-Design Pro, 2000, Solar Design Studio, v4.0, Maui Solar Energy Software Corp., Haiku, HI.
- [15] King, D. L., Kratochvil, J. A., and Boyson, W. E., 1997, "Temperature Coefficients for PV Modules and Arrays: Measurement Methods, Difficulties, and Results," *Proc. 26th IEEE Photovoltaic Specialists Conference*, Anaheim, CA, September 29–October 3, pp. 1183–1186.
- [16] King, D. L., 1996, "Photovoltaic Module and Array Performance Characterization Methods for All System Operating Conditions," *Proc. NREL/SNL Photovoltaics Program Review*, New York, AIP Press, Lakewood, CO, November 18–22, pp. 347–368.
- [17] King, D. L., Kratochvil, J. A., and Boyson, W. E., 1997, "Measuring Solar Spectral and Angle-of-Incidence Effects on Photovoltaic Modules and Solar Irradiance Sensors," *Proc. 26th IEEE Photovoltaic Specialists Conference*, Anaheim, CA, September 29–October 3, pp. 1113–1116.
- [18] ASTM E 1036-02, "Standard Test Methods for Electrical Performance of Non-concentrator Terrestrial Photovoltaic Modules and Arrays Using Reference Cells," *Annual Book of ASTM Standards*, Vol. 12.02.
- [19] Myers, D. R., and Emery, K., 2002, "Terrestrial Solar Spectral Modeling Tools and Applications for Photovoltaic Devices," *IEEE* 2002, May 20–24, pp. 1683–1686.
- [20] Kasten, F., and Young, T., 1989, "Revised Optical Air Mass Tables and Approximation Formula," *Appl. Opt.* **28**(22), pp. 4735–4738.
- [21] Duffie, J. A., and Beckman, W. A., 1991, *Solar Engineering of Thermal Processes*, John Wiley and Sons, New York.
- [22] Martin, N., and Ruiz, J. M., 2005, "Annual Angular Reflection Losses in PV Modules," *Prog. Photovoltaics* **13**, pp. 75–84.
- [23] King, D. L., Kratochvil, J. A., and Boyson, W. E., 1998, "Field Experience with a New Performance Characterization Procedure for Photovoltaic Arrays," *Proc. 2nd World Conference and Exhibition on Photovoltaic Solar Energy Conversion*, Vienna, Austria, July 6–10.
- [24] ASTM G 159-98, "Standard Tables for References Solar Spectral at Air Mass 1.5: Direct Hemispherical for a 37° Tilted Surface," *Annual Book of ASTM Standards*, Vol. 14.04.
- [25] ASTM E 973-02, "Determination of the Spectral Mismatch Parameter Between a Photovoltaic Device and a Photovoltaic Reference Cell," *Annual book of ASTM Standards*, Vol. 12.02.
- [26] Whitfield, K., and Osterwald, C. R., 2001, "Procedure for Determining the Uncertainty of Photovoltaic Module Outdoor Electrical Performance," *Prog. Photovoltaics* **9**, pp. 87–102.
- [27] Fanney, A. H., and Dougherty, B. P., 2001, "Building Integrated Photovoltaic Test Facility," *Sol. Energy* **123**, pp. 200–210.